

RESEARCH ARTICLE

Economical Setting-Free Double-Ended Fault Locator for Transmission Lines: Experiences From Recent Pilot Installations

O. D. NAIDU¹, (Senior Member, IEEE), SINISA ZUBIC², A. V. S. S. R. SAI¹,
A. N. PRAVEEN¹, PATRICK COST², AND HÅKAN ERIKSSON³

¹Hitachi Energy, Grid Automation, Bengaluru, Karnataka 560048, India

²Hitachi Energy, Grid Automation, 72159 Västerås, Sweden

³Svenska Kraftnät (SVK), 172 24 Sundbyberg, Sweden


Corresponding author: O. D. Naidu (od.naidu@hitachienergy.com)

ABSTRACT Locating fault precisely on power transmission line is highly beneficial to utilities and accurate fault location can expedite the repair of the faulted components, speed-up restoration, and reduce outage time. In this paper, a *setting-free* double ended fault location method for power transmission line is proposed using both end voltage and current measurements. This algorithm estimates the required setting parameters using pre-fault data and fault location is calculated using estimated parameters and during fault data. The proposed method is verified using the EMTDC simulations for lines connected with conventional and inverter-based renewable resources. The method is not affected by the error in line parameters and renewable integration. The method is implemented in Intelligent Electronic Device (IED) using 1kHz sampling rate and successfully installed on a 400 kV, 233.07 km line from Power Grid Corporation of India (POWERGRID), India and on a 220 kV, 265.6 km line from Svenska Kraftnat (SVK), Sweden. This paper presents laboratory test results as well as field experimental results in which line patrolling crews found the actual location. Pilot installation results match the performance demonstrated with laboratory experimental results. The method gives average fault location error of $\sim 0.1\%$. The method can locate the fault within two-tower span distance ($\sim 300\text{m}$) which is comparable with traveling wave-based method that requires 1000 times higher sampling rate, high-cost hardware, more complex commissioning, and settings. These geographically diverse pilot installation results stand as testimony to the fault location accuracy of the proposed setting-free fault location solution.

INDEX TERMS Impedance-based fault locator, inverter-based renewable resources, line fault, parameter estimation, renewables, setting free fault location, transmission lines.

I. INTRODUCTION

Power transmission lines are exposed to faults due to bad weather (hurricanes, lightnings), insulation breakdown, short circuits by birds, contacting tree branches with a transmission line and other objects. Temporary faults are cleared by auto-reclosing. For permanent faults, the power supply is restored only after the maintenance crew detects and replaces the failed component. For this purpose, precise fault location should be known, else, the fault location identification job

The associate editor coordinating the review of this manuscript and approving it for publication was Ali Raza .

turns out to be tedious and time consuming for long transmission lines spread across rugged terrains such as hilly areas, mountains, and deserts etc. [1], [2]. Visual inspection techniques are advanced from road patrols to air patrols and, more recently, to trials with drones and unmanned aerial vehicles etc. and these methods may not be cost effective for long transmission lines.

Identification of fault location with high precision on power transmission line is of great value to transmission asset owners and maintenance crew as it helps in expediting maintenance work and achieving quick restoration of the line [2]. Quick restoration of service improves the reliability of

power supply and reduces the financial loss for the utilities and end users [3].

Traveling wave (TW)-based fault locators are used to locate the fault within 1-2 towers span distance [4], [5], [6], [7], [8], [9], [10], [11], [12], [13], [14], [15]. The performance of TW based fault location (FL) methods depends on accurate detection of wavefront arrival times, sampling rate, and data synchronization [4]. Based on the availability of input to fault locator, traveling wave-based methods can be classified into two types viz. 1) single-ended [5], [6], [7], [8], and 2) double-ended [4], [9], [10], [11], [12], [13], [14], [15]. The single-ended TW-based methods use the incident and reflected wave arrival times to locate the fault. The single-ended TW-based techniques pose challenges in identifying the waves reflected from the location of the fault and the remote substation terminals, as well as the waves reflected from the buses of adjacent networks connected to the protected line [5], [8]. Therefore, the practical implementation of the single-ended TW-methods is challenging and limited.

Double-ended TW-based methods [9], [10], [11], [12], [13], [14], [15] are more accurate and these methods are in practical usage [4], [10], [11], [12]. However, accuracy of TW-based FL algorithms depends on traveling wave detection, data synchronization, IED hardware, processing of multiple reflections, filtering of noise, correction of substation secondary cable delays [13], and wave speed [14], etc. These data synchronization and wave speed errors can be corrected by conducting experiments [15] such as creating a fault at known distance and calculating the secondary cable delays and wave speed. This process is difficult, requires more engineering effort and not cost-effective. Besides, they are not economical solutions for transmission asset owners due to the high cost involved in dedicated hardware and solution tuning efforts.

Impedance-based FL methods are most employed by transmission system operators (TSOs) because of ease of use, low sampling rate data requirement, and low hardware cost [2], [3]. These methods are classified into two types viz. 1) Single-ended [16], [17], [18], [19], [26], [27], and 2) Double-ended [28], [29], [30], [31], [32], [33], [34], [35]. The single-ended methods are commonly available as an inbuilt function in the protection IEDs and not required any communication and GPS [2], [19]. However, the precision of single-ended FL algorithms [20], [21], [22] is influenced by the type of fault, arc resistance, impedance angles of line and source, mutual compensation, uncertainty of the line parameters, and system non-homogeneity. As a result, the accuracy of the commercially available single-ended impedance-based fault locators are in the order of 1.5 to 2.5 percent. For a 300-kilometer transmission line, a ± 1.5 percent error still requires 9-kilometer length to be inspected (about 30 towers) which is not cost-effective.

And also, the main assumption of single-ended fault locator techniques is that the fault current at the FL is in phase with fault current at the terminals [16] and in phase with negative

sequence current at the terminal [20]. These assumptions may not hold for lines connected with inverter-based renewables resources as the phase angle is modulated by the inverter controls and grid codes [23], [24], [25]. The single-ended fault location principles are greatly affected with the integration of renewables [25]. During fault, the controlled phase angle of inverter-based resources (IBRs) current introduces the high non-homogeneity in impedance calculation [25]. This in turn causes large error in the apparent impedance calculation, especially for resistive faults. This results in the calculated fault location to be lesser or more than the actual fault location value. Therefore, single-ended FL methods will not provide the desirable FL accuracy for lines connected with renewable power plants [25].

A single-ended-fault location method for grid-connected converter system based on control and protection coordination is presented in [26]. A single-terminal fault location method for transmission lines integrated by the inverter-type source is proposed in [27]. These methods use the converter control information in fault location formulation and solves the fault location iteratively. These methods may not be easy to implement in IEDs as they require control information of the inverters.

Present communication technology allows for use of data from both ends of the line to calculate the location of the fault [2]. The accuracy of double-ended methods [30], [31] is not affected by fault resistance, loading, fault loop information, and system non-homogeneity. These methods are economical alternative to traveling wave-based methods that requires high sampling rates. Rearrangement method of reducing fault location error in tied uncompleted parallel lines is presented in [32]. A robust fault location method using sparse set of digital fault recorders for radial or meshed power networks is presented in [33]. This method requires network level data which is not available in IEDs. The negative sequence-based methods are more advantageous as they are not affected by load current and zero sequence impedance [34], [35]. However, these methods may not be suitable for lines connected with converter interfaced renewable power plants (CIRPPs) as most of these plants will not supply negative sequence current [23], [24], [25]. The positive-sequence impedance-based algorithms are used to locate the faults for lines connected with CIRPPs since positive sequence quantities are available for lines connected with conventional sources and CIRPPs. There are several fault location methods for transmission lines reported in literature [1], [28], [29], [30], [31], [32], [33], [34], [35] for utilizing synchronized measurements from both ends. The accuracy of the two-ended impedance-based fault location algorithms depend on the accuracy of line parameters such as inductance, capacitance, and resistance. The electrical parameters of a transmission line are not known with great precision. It is noted in case studies that there is up to 25-30% of error in actual and the stored values of the line parameters [36]. Line parameter with little accuracy is sufficient for protection applications but for accurate FL, precise line parameters are required. These line parameters

are not constant and varies with practical conditions such as weather, age of the conductor etc.

The line parameters estimation may help to improve the accuracy of the double-ended fault location. Several methods have been proposed for line parameter estimation for transmission lines [37], [38], [39], [40], [41], [42], [43], [44], [45]. The online tracking of line parameter using SCADA data is proposed in [37] and this technique requires multiple measurement sets. In [38], multiple measurement scans are used with Lagrangian multipliers for improving the accuracy of the line parameter estimation. A more accurate calculation of the transmission line parameters can be performed by using synchronized current and voltage phasor measurements provided by the PMUs [39], [40] and these methods require multiple data sets which may not be available all the time and it is difficult implement in IED platforms. To mitigate requirement of multiple data set, a method to estimate the parameters estimation for three-terminal mixed line using pre and during fault phasors is presented in [41]. This method requires the negative sequence currents, and it will not work for lines connected with CIRPPs. Impedance estimation method for transmission line by assuming linearly changing parameters for short periods is presented in [42]. A technique for estimation of electrical parameter of transmission line using synchronized sampled data proposed in [43]. This method can obtain the steady state values of voltage and current of the transmission line as a function of time and line length. In [44], Kalman filter (KF) and extended Kalman filter (EKF) have been applied for state and parameter estimation of non-uniform transmission line. A stochastic based state equations are derived using Telegrapher's equation for transmission line. Nonlinearities in line voltage and current have been taken into account by implementing perturbation theory. A data driven based method for detection and identification of line parameters of a transmission line is presented in [45] using PMU and unsynchronized SCADA measurements. Data driven methods may not be suitable for implementation in IED platforms. From the literature review, there is a scope for improvement in double-ended fault locator accuracy by eliminating the dependency on parameters and settings.

In this paper, a *setting-free* fault location method for transmission lines using double-ended data is proposed. This algorithm estimates the required setting parameters using pre-fault data and fault location is calculated using estimated parameters, and during fault phasors. The proposed algorithm aims to estimate the line parameters using a two-step approach using one set of pre-fault data. Line parameters are calculated using lumped line model in step one. In second step, the parameters obtained from step one is given as initial guess and the nonlinear equations formulated using distributed parameter line model are solved. The FL is calculated using the estimated parameters and during fault phasors.

The proposed method does not require information about line parameters or settings and saves the engineering cost of the solution. The main contributions of this work are as follows:

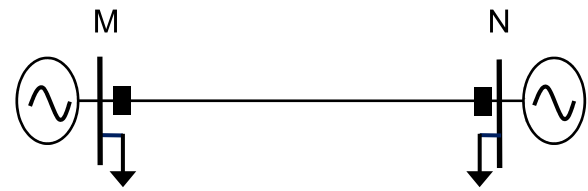


FIGURE 1. Two terminal transmission line single line diagram.

(i) parameter estimation using single set of pre-fault data, (ii) fault location calculation using during fault data, (iii) implementation in IED platform, (iv) experimental validation using two pilot installations in Indian and Swedish grid.

The proposed algorithm is verified through the EMTDC simulations covering various fault scenarios for 220-kV, 240 km line connected with conventional and inverter-based renewables resources. The method is implemented in IED and successfully commissioned on a 400-kV 233.07 km line from Power Grid Corporation of India (POWERGRID), India and on a 220 kV 256.6 km line from Svenska Kraftnat (SVK), Sweden. The parameter estimation and fault location algorithm, hardware, software requirements, experimental setup, and results are provided in this paper. The simulation and experimental results are consistent, and the proposed algorithm can locate the fault within two-tower span distance using 1kHz sampling data which is comparable with traveling wave-based methods that requires thousand times ($\sim 1\text{MHz}$) higher sampling rates. The proposed method does not require information about line parameters or settings, saves on engineering cost and does not require any additional hardware beyond what is required for a modern line differential protection solution [47], i.e., a 2 Mbps communication link.

II. PROPOSED METHOD

The paper is organized as follows: (i) parameter estimation, (ii) fault location formulation, (iii) implementation in IED platform, (iv) simulation result studies for lines connected with conventional generation and renewable power plants, (v) pilot installation in Indian and Swedish grid, and (viii) conclusions. The details of the modules are provided below.

A. PROPOSED PARAMETER ESTIMATION METHOD

This section describes the details of the line parameter estimation algorithm using a two-step approach. In step one, line parameters are calculated using a lumped model of the line. In step two, the line parameters obtained from step one is given as an initial guess to the least-squares method and the accurate line parameters are estimated using complete model (distributed parameter model). The entire approach requires one set of measurement data (pre-fault) only. The details are provided as below.

1) INITIAL GUESS CALCULATION USING LUMPED MODEL OF THE LINE

Consider a transmission line connected between buses M and N as shown in Fig.1 and two-port lumped π model as shown

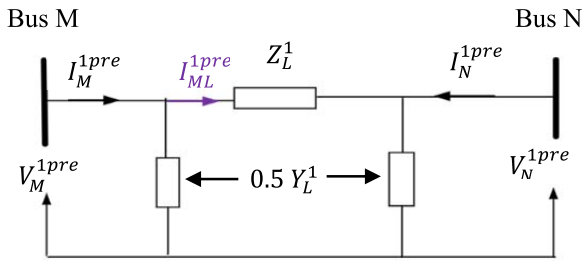


FIGURE 2. Two terminal transmission line lumped model.

Fig.2. From Fig.2, the fault current flowing in the series impedance (I_{ML}^{1pre}) is calculated from bus M and N as in (1) and (2) respectively.

$$I_{ML}^{1pre} = I_M^{1pre} - \frac{l_{MN}}{2} (Y_L^1) (V_M^{1pre}) \quad (1)$$

$$I_{ML}^{1pre} = -I_N^{1pre} + \frac{l_{MN}}{2} (Y_L^1) (V_N^{1pre}) \quad (2)$$

where, V_M^{1pre} and V_N^{1pre} are pre-fault positive sequence voltage measured at bus M and N respectively; I_M^{1pre} and I_N^{1pre} are pre-fault positive sequence current measured at bus M and N respectively; I_{ML}^{1pre} is pre-fault current flowing through series impedance; Z_L^1 and Y_L^1 are positive sequence series impedance and shunt admittance per meter of the line respectively and l_{MN} is the length of the line in meters.

Line admittance is obtained as in (3) using (1) and (2),

$$Y_L^1 = \frac{2}{l_{MN}} \left(\frac{I_M^{1pre} + I_N^{1pre}}{V_M^{1pre} + V_N^{1pre}} \right) \quad (3)$$

From Fig.2, we have,

$$V_M^{1pre} - V_N^{1pre} = I_{ML}^{1pre} l_{MN} Z_L^1 \quad (4)$$

Substitute I_{ML}^{1pre} and Y_L^1 in (4), we get (5)

$$V_M^{1pre} - V_N^{1pre} = \left(I_M^{1pre} - \left(\frac{I_M^{1pre} + I_N^{1pre}}{V_M^{1pre} + V_N^{1pre}} \right) V_M^{1pre} \right) l_{MN} Z_L^1 \quad (5)$$

Series impedance can be obtained as in (6) after simplification of (5)

$$Z_L^1 = \frac{1}{l_{MN}} \left(\frac{(V_M^{1pre})^2 - (V_N^{1pre})^2}{V_N^{1pre} I_M^{1pre} - V_M^{1pre} I_N^{1pre}} \right) \quad (6)$$

Line parameters are obtained using the following relations:

$$R^1 = \text{real}(Z_L^1); \quad L^1 = \frac{\text{imag}(Z_L^1)}{2\pi f}; \quad C^1 = \frac{\text{imag}(Y_L^1)}{2\pi f}$$

where,

R^1 , L^1 , C^1 are positive sequence resistance, inductance, and capacitance per meter of the transmission line respectively; f is system frequency in Hz. These parameters obtained using the simplified lumped model of the line are used as initial guess in the next step.

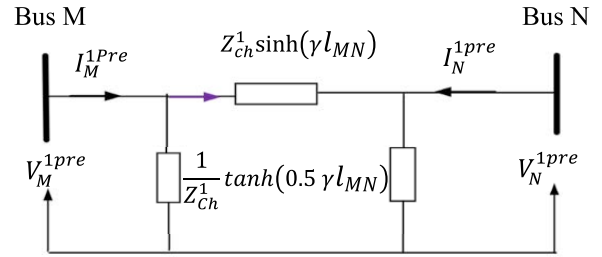


FIGURE 3. Two terminal transmission line distributed model.

2) LINE PARAMETER ESTIMATION USING DISTRIBUTED MODEL OF THE LINE

In this section, the line parameters are estimated using the distributed model of the line as shown in Fig.3. The objective functions are formulated using the basic two-port network relationships.

From the two-port network shown in Fig.3, we have,

$$V_M^{1pre} = V_N^{1pre} \cosh(\gamma l_{MN}) - I_N^{1pre} Z_{ch}^1 \sinh(\gamma l_{MN}) \quad (7)$$

$$I_M^{1pre} = \frac{V_N^{1pre}}{Z_{ch}^1} \sinh(\gamma l_{MN}) - I_N^{1pre} \cosh(\gamma l_{MN}) \quad (8)$$

where,

$$Z_{ch}^1 = \sqrt{\frac{Z_L^1}{Y_L^1}} \quad \gamma = \sqrt{Z_L^1 \times Y_L^1};$$

$$Z_{ch}^1 = \text{Characteristic impedance of the line}$$

$$\gamma = \text{propagation constant of the line}$$

The non-linear equations (7) and (8) are solved by using least square estimation technique to obtain the actual line parameters of the line. The initial guess required for this solution is obtained from the previous step. The detailed steps for solving these equations are mentioned in the previously published paper [46]. The line parameters are obtained by solving the objective functions (7) and (8). This is under-determined problem with set of two equations to solve for four unknowns and that cannot be solved directly. Now let us separate objective function in to real and imaginary parts as in (9) and (10),

$$V_{Mr}^{1pre} + jV_{Mi}^{1pre} = (V_{Nr}^{1pre} + jV_{Ni}^{1pre}) \cosh(a + jb) - (c + jd) \times \sinh(a + jb) \times (I_{Nr}^{1pre} + jI_{Ni}^{1pre}) \quad (9)$$

$$I_{Mr}^{1pre} + jI_{Mi}^{1pre} = (V_{Nr}^{1pre} + jV_{Ni}^{1pre}) \frac{\sinh(a + jb)}{(c + jd)} - (I_{Nr}^{1pre} + jI_{Ni}^{1pre}) \cosh(a + jb) \quad (10)$$

where,

$Z_{ch}^1 = c + jd$; $\gamma l_{MN} = a + jb$; $V_M^{1pre} = V_{Mr}^{1pre} + jV_{Mi}^{1pre}$; $I_M^{1pre} = I_{Mr}^{1pre} + jI_{Mi}^{1pre}$; $V_N^{1pre} = V_{Nr}^{1pre} + jV_{Ni}^{1pre}$; $I_N^{1pre} = I_{Nr}^{1pre} + jI_{Ni}^{1pre}$; $V_{Mc}^{1pre} = V_{Mcr}^{1pre} + jV_{Mci}^{1pre}$; $I_{Mc}^{1pre} = I_{Mcr}^{1pre} + jI_{Mci}^{1pre}$ and suffix ‘‘r’’ and ‘‘i’’ represents the real and imaginary quantities.

Elaborating the hyperbolic functions, we get (11) and (12)

$$\begin{aligned} \cosh(a + jb) &= \cosh(a) \times \cos(b) + j \sinh(a) \times \sin(b) \\ &= +jq \end{aligned} \quad (11)$$

$$\begin{aligned} \sinh(a + jb) &= \sinh(a) \times \cos(b) + j \cosh(a) \times \sin(b) \\ &= r + js \end{aligned} \quad (12)$$

Substituting (11) and (12) in (9) and (10), we get

$$\begin{aligned} V_{Mr}^{1pre} + jV_{Mi}^{1pre} &= (V_{Nr}^{1pre} + jV_{Ni}^{1pre})(p + jq) \\ &\quad - (c + jd)(r + js) \times (I_{Nr}^{1pre} + jI_{Ni}^{1pre}) \end{aligned} \quad (13)$$

$$\begin{aligned} I_{Mr}^{1pre} + jI_{Mi}^{1pre} &= (V_{Nr}^{1pre} + jV_{Ni}^{1pre}) \frac{(r + js)}{(c + jd)} \\ &\quad - (I_{Nr}^{1pre} + jI_{Ni}^{1pre})(p + jq) \end{aligned} \quad (14)$$

Separating real and imaginary parts, we get

$$\begin{aligned} V_{Mr}^{1pre} &= pV_{Nr}^{1pre} - qV_{Ni}^{1pre} (cI_{Nr}^{1pre} - dI_{Ni}^{1pre})r \\ &\quad + (cI_{Ni}^{1pre} + dI_{Nr}^{1pre})s \end{aligned} \quad (15)$$

$$\begin{aligned} V_{Mi}^{1pre} &= pV_{Ni}^{1pre} - qV_{Nr}^{1pre} (cI_{Nr}^{1pre} - dI_{Ni}^{1pre})s \\ &\quad - (cI_{Ni}^{1pre} + dI_{Nr}^{1pre})r \end{aligned} \quad (16)$$

$$\begin{aligned} I_{Mr}^{1pre} &= \frac{cr + ds}{c^2 + d^2} V_{Nr}^{1pre} ((cs - dr)/(c^2 + d^2)) V_{Ni}^{1pre} \\ &\quad - pI_{Nr}^{1pre} + qI_{Ni}^{1pre} \end{aligned} \quad (17)$$

$$\begin{aligned} I_{Mi}^{1pre} &= \frac{cr + ds}{c^2 + d^2} V_{Ni}^{1pre} + \left(\frac{cs - dr}{c^2 + d^2} \right) V_{Nr}^{1pre} \\ &\quad - pI_{Ni}^{1pre} - qI_{Nr}^{1pre} \end{aligned} \quad (18)$$

Four non-linear equations (15)-(18) of the form $F(X) = 0$, where $F = (f1, f2, f3, f4)^T$ and $X = (a, b, c, d)^T$, are solved for the four unknowns using the least square estimation (LSE) method.

For the non-linear set of equations $F(X) = 0$,

$$s = - (H^T H)^{-1} H^T F \quad (19)$$

where, H is the Jacobian matrix.

Therefore equation (19) can be written as-

$$\begin{aligned} \begin{bmatrix} \Delta a \\ \Delta b \\ \Delta c \\ \Delta d \end{bmatrix} &= - \left(\begin{bmatrix} H_{11} & \dots & H_{14} \\ \vdots & \ddots & \vdots \\ H_{41} & \dots & H_{44} \end{bmatrix}^T \begin{bmatrix} H_{11} & \dots & H_{14} \\ \vdots & \ddots & \vdots \\ H_{41} & \dots & H_{44} \end{bmatrix} \right)^{-1} \\ &\quad \times \begin{bmatrix} H_{11} & \dots & H_{14} \\ \vdots & \ddots & \vdots \\ H_{41} & \dots & H_{44} \end{bmatrix}^T \begin{bmatrix} f1 \\ f2 \\ f3 \\ f4 \end{bmatrix} \end{aligned} \quad (20)$$

where,

$$\begin{aligned} f1 &= V_{Mr}^{1pre} V_{Mcr}^{1pre}; & f2 &= V_{Mi}^{1pre} V_{Mci}^{1pre}; \\ f3 &= I_{Mr}^{1pre} I_{Mcr}^{1pre}; & f4 &= I_{Mi}^{1pre} I_{Mci}^{1pre} \end{aligned}$$

The updated value of variable matrix, X in next iteration is-

$$X = X(0) + s \quad (21)$$

Initial guess $X(0)$ is obtained from step one.

$$\begin{bmatrix} a \\ b \\ c \\ d \end{bmatrix} = \begin{bmatrix} a_0 \\ b_0 \\ c_0 \\ d_0 \end{bmatrix} + \begin{bmatrix} \Delta a \\ \Delta b \\ \Delta c \\ \Delta d \end{bmatrix} \quad (22)$$

The final parameters are determined using the following relationships.

$$\begin{aligned} Z_{ch}^1 &= c + jd; & \gamma &= (a + jb)/l_{MN}; \\ \omega &= 2\pi f; & Z_L^1 &= Z_{ch}^1 \times \gamma = R^1 + jX^1; \\ Y^1 &= \gamma/Z_{ch}^1 = G^1 + jB^1; & R^1 &= \text{Re}(Z_L^1); \\ L^1 &= \text{Im}(Z_L^1)/\omega; & C^1 &= \text{Im}(Y_L^1)/\omega. \end{aligned}$$

These estimated parameters are used as an input for fault locator method which is described in the next section.

B. DOUBLE ENDED FAULT LOCATION METHOD

This section presents a fault location method for two-terminal lines using both end measurements. The idea is derived from [46] and is developed into a *setting free* fault location formulation. The main idea is that the fault location formulation is derived by equating the fault point voltage calculated from both ends of the line. Consider a two-terminal transmission line with two IEDs, and each one installed at the terminals of the transmission line. Let us consider a-g fault on the transmission line at a distance 'd' from the terminal M.

Calculate the fault point voltage and current using ABCD parameters from terminal M

$$\begin{bmatrix} V_{FM}^{1f} \\ I_{FM}^{1f} \end{bmatrix} = \begin{bmatrix} D_d^1 & -B_d^1 \\ -C_d^1 & A_d^1 \end{bmatrix} \begin{bmatrix} V_M^{1f} \\ I_M^{1f} \end{bmatrix} \quad (23)$$

From (23), calculate the fault point voltage from terminal M as in (24)

$$V_{FM}^{1f} = D_d^1 V_M^{1f} - B_d^1 I_M^{1f} \quad (24)$$

where, positive sequence A_d^1, B_d^1, C_d^1 , and D_d^1 parameters are defined up to fault point 'd' and ABCD parameters are calculated as in (25).

$$\begin{aligned} A_d^1 &= D_d^1 = \cosh(\gamma dl_{MN}); & B_d^1 &= Z_{ch}^1 \sinh(\gamma dl_{MN}); \\ C_d^1 &= \frac{1}{Z_{ch}^1} \sinh(\gamma dl_{MN}) \end{aligned} \quad (25)$$

Similarly, calculate the fault point voltage and current from terminal N as in (26)

$$V_{FN}^{1f} = D_{1-d}^1 V_N^{1f} - B_{1-d}^1 I_N^{1f} \quad (26)$$

where ABCD parameters are defined as in (27)

$$\begin{aligned} A_{1-d}^1 &= D_{1-d}^1 = \cosh(\gamma l_{MN}(1 - d)); \\ B_{1-d}^1 &= Z_{ch}^1 \sinh(\gamma l_{MN}(1 - d)); \\ C_d^1 &= \frac{1}{Z_{ch}^1} \sinh(\gamma l_{MN}(1 - d)) \end{aligned} \quad (27)$$

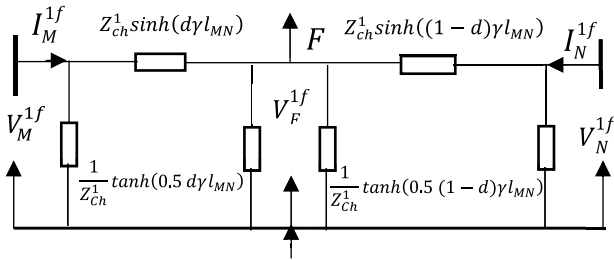


FIGURE 4. Positive sequence network during fault.

Substitute (25) in (24) and (27) in (26), we get (28)

$$\begin{aligned} V_{FM}^{1f} &= V_M^{1f} \cosh(\gamma dl_{MN}) - I_M^{1f} Z_{ch}^1 \sinh(\gamma dl_{MN}); \\ V_{FN}^{1f} &= V_N^{1f} \cosh(\gamma l_{MN}(1-d)) - I_N^{1f} Z_{ch}^1 \sinh(\gamma l_{MN}(1-d)) \end{aligned} \quad (28)$$

Expand the cosh and sinh terms and equate the fault point voltages calculated from both terminals as in (29)

$$\begin{aligned} V_M^{1f} \cosh(\gamma dl_{MN}) - I_M^{1f} Z_{ch}^1 \sinh(\gamma dl_{MN}) \\ = V_N^{1f} (\cosh(\gamma l_{MN}) \cosh(\gamma l_{MN} d) \\ - \sinh(\gamma l) \sinh(\gamma l_{MN} d)) - (I_N^{1f} Z_{ch}^1) (\sinh(\gamma l_{MN}) \\ \times \cosh(\gamma l_{MN} d) - \cosh(\gamma l_{MN}) \sinh(\gamma l_{MN} d)) \end{aligned} \quad (29)$$

Fault location is obtained as in (30) from (29)

$$d = \frac{1}{\gamma l_{MN}} \tanh^{-1} \left(\frac{K_1}{K_2} \right) \quad (30)$$

where, $K_1 = V_N^{1f} \cosh(\gamma l_{MN}) + (I_N^{1f} Z_{ch}^1) (\sinh(\gamma l_{MN}) - V_M^{1f})$, $K_2 = V_N^{1f} \sinh(\gamma l_{MN}) - (I_N^{1f} Z_{ch}^1) (\cosh(\gamma l_{MN}) - Z_{ch}^1 I_M^{1f})$, $Z_{ch}^1 = \sqrt{(R^1 + j\omega L^1) / (j\omega C^1)}$;

$\gamma = \sqrt{(R^1 + j\omega L^1) (j\omega C^1)}$, R^1 , L^1 and C^1 are resistance, inductance and capacitance per unit length of the line which are estimated using the pre-fault voltage and current measured at both ends of the line. The proposed method does not require any settings to locate the fault. The complete algorithm steps are depicted in the flow diagram shown in Fig.5. The proposed method is implemented in IED [47] platform using 1kHz sampling rate. The practical implementation, communication network and data synchronization details are provided below.

III. SIMULATION RESULTS AND ANALYSIS

This section provides the illustrative examples, detailed study on effect of variation in power system parameters on FL accuracy, comparative assessment with existing practically available methods, and results for lines connected with inverter-based renewables resources.

A. SIMULATION STUDY FOR LINES CONNECTED WITH CONVENTIONAL SOURCES

To test and illustrate the validation of the method in the previous section, EMTDC/PSCAD has been used to simulate the

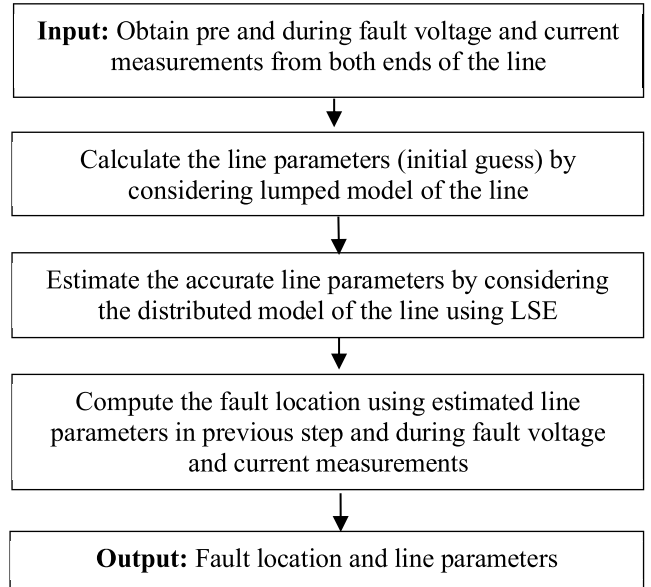


FIGURE 5. Flow chart of the proposed setting-free fault location.

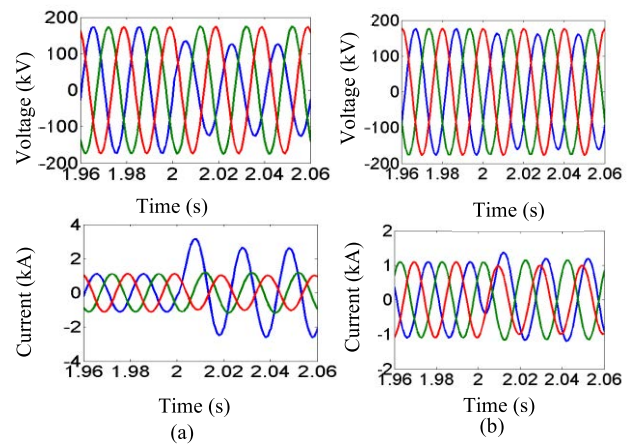


FIGURE 6. Pre and during fault voltage and current signals measured at (a) Bus M and (b) Bus N for a-g fault at 60km from M.

faults on a 220-kV, 50Hz, 240km two-terminal transmission line. The simulations are done in the EMTDC software with frequency dependent transmission line models. The fault data is recorded as COMTRADE99 format and Discrete Fourier Transform (DFT) is applied to obtain the current and voltage phasors. The main inputs to the algorithm are synchronized pre and during fault voltage and current phasors and line length.

1) ILLUSTRATIVE CASE

A-g fault case: Consider a-g fault at 60km from bus M on the transmission line with fault resistance of 25Ω, fault inception angle is 0 degree and source to line impedance ratio (SIR) is 1.0. The voltage and current signals are as shown in the Fig.6.

The calculated (lumped model) and estimated (distributed line model) line parameters and corresponding errors

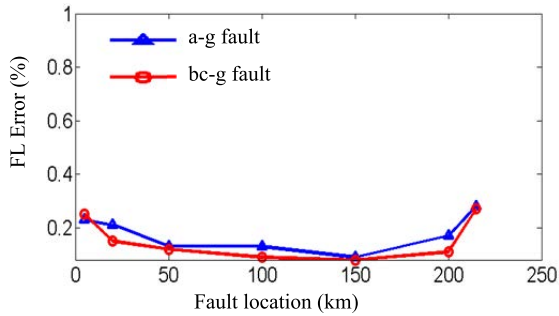


FIGURE 7. Fault location errors for different fault locations for a-g and bc-g faults.

TABLE 1. Calculated line parameters using lumped model.

Method	R^1 (Ω /KM)	L^1 (mH/KM)	C^1 (NF/KM)
Actual	0.1879	1.03870	16.18147
Proposed	0.1838	1.02739	16.27543
Error (%)	2.18	1.10	0.58

TABLE 2. Estimated line parameters using distributed line model.

Method	R^1 (Ω /KM)	L^1 (mH/KM)	C^1 (NF/KM)
Actual	0.1879	1.03870	16.18147
Proposed	0.1880	1.03878	16.18532
Error (%)	0.02	0.01	0.02

compared to actual line parameters for this case are provided in the Table 1 and 2 respectively. From Table 1 and 2, the calculated and estimated parameters are close to actual parameters. The estimated parameters are more accurate than calculated and these parameters are used for fault location calculation. The calculated fault location using the estimated line parameters and post fault phasors is 59.85 km. The absolute percentage of fault location error calculated using (31) is 0.06% for the 240 km transmission line for this case.

$$\%Error = \left| \frac{\text{Actual Fault Location} - \text{Calculated Fault Location}}{\text{The total length of the line}} \right| \times 100 \quad (31)$$

B. STUDY ON EFFECTIVENESS OF THE PROPOSED METHOD FOR VARIOUS FAULT CONDITIONS

This section presents the effectiveness of the proposed method on variation of different fault conditions (i) influence caused by fault location, (ii) effect of fault resistance, and (iii) effect of source to line impedance ratios (SIRs). The results are provided below.

1) STUDY OF THE INFLUENCE CAUSED BY FAULT LOCATION

This section provides the results for effect of variation fault location on the proposed method. Location of the fault is one of the negative effects on impedance-based fault location methods [21]. In this section, various fault locations (5, 20,

TABLE 3. Study of effect of fault resistance variation on proposed method.

Fault Type	R_F (Ω)	Max.FL Error (%)	Avg.FL Error (%)
a-g	0.01	0.19	0.09
	5	0.18	0.10
	10	0.23	0.10
	50	0.31	0.11
	100	0.37	0.12
bc-g	0.01	0.14	0.07
	5	0.13	0.09
	10	0.17	0.10
	50	0.27	0.10
	100	0.31	0.11

50, 100, 150, 200 and 215 km) are considered to test the effect of fault distances on the proposed solution. Phase a-to-ground (a-g) and double phase to ground (bc-g) faults are considered. In the simulation, the values of the fault inception and fault resistance are set to 60^0 and 10Ω respectively. The same simulation system described in the Section A is used for simulations. Fig.7 shows the performance of the proposed solution with different fault distances for two types of the faults. The FL errors are less than 0.3% and observed slightly high fault location error for faults closer to fault locator due to high DC component in the voltage and current signals. High DC components in the fault signals affects the estimation of the voltage and current phasors.

2) STUDY OF THE EFFECT OF FAULT RESISTANCE ON THE PROPOSED METHOD

Fault resistance (R_F) is one of the most negative influences on the impedance-based fault location methods [21]. To evaluate the performance of the proposed method with various fault resistances, various values of fault resistances 0.1Ω , 5Ω , 10Ω , 50Ω , and 100Ω , have been considered. The source impedance parameters are kept constant, and the fault locations are varied from 10-240 km with an interval of 10km for a-g and bc-g faults. A total of 240 cases are simulated. Table 3 shows the maximum and average fault location errors for various fault resistances. The maximum FL error is 0.37% when fault resistance is 100Ω for a-g fault. The average error is 0.1% which is acceptable. The results show that the accuracy of the proposed method does not change notably with change in fault resistance.

3) STUDY OF THE EFFECT OF SOURCE TO LINE IMPEDANCE RATIO ON THE PROPOSED METHOD

The source strength is adversely impacting the impedance-based FL methods [21]. In this section, two source to line impedance ratios (SIRs) are considered to verify the performance of the proposed method. Various FLs (5, 20, 50, 100, 150, 200 and 235 km) and two fault types (a-g and bc) are considered for EMTDC simulations. In the simulation, the values of the fault inception and fault resistance are set to 60^0 and 20Ω respectively. Fig.8 shows the performance of

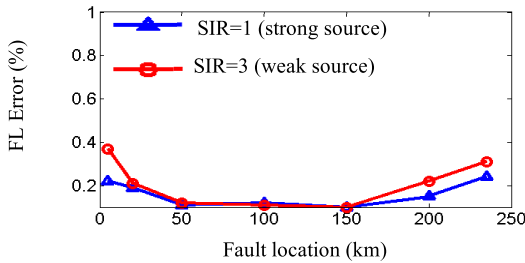


FIGURE 8. Fault location errors for different source to line impedance ratio for a a-g fault.

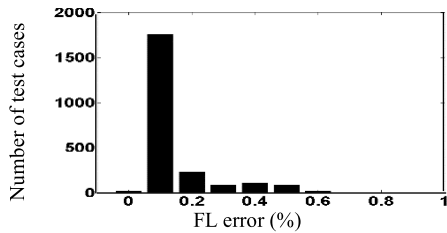


FIGURE 9. Performance of the proposed fault location method for various fault situations.

TABLE 4. Fault situations considered for simulation study.

Test Cases	Test conditions
Fault Location (km)	1, 60, 120, 100 180 and 235
Fault Type	a-g, ab, bc-g and abc-g
Fault Inception Angle	0° and 90°
Fault resistance (Ω)	0.01, 10, 20 and 50
SIR (M:N)	0.1:1, 1:2, 2:3 and 5:2
Load	No load (0%), 100 % and 125%

the proposed solution with different source to line impedance ratios (1 and 3) for phase a to ground faults. The FL error notably increases with increase in SIR for faults closer to terminals of the line due to high transients in fault signals. High transients will affect the phasor estimation for faults closer to line terminals with high source to line impedance ratios. The maximum FL error observed is 0.37% for high SIR case which is acceptable accuracy

C. DETAILED STUDY USING VARIOUS TEST CONDITIONS

The proposed method is tested with different power system fault situations. The fault situations are tabulated in Table 4. Total 2304 fault cases are tested, and fault location error is presented in Fig.9.

From figure 9, the average and maximum fault location errors are 0.1% and 0.6% respectively. The fault location error is 0.1% (~240m) for 1756 (76.21%) cases which is less than one tower span (300m) distance for a 240km line. The accuracy is comparable to traveling wave-based fault locators [9], [10], [11], [12], [13], [14] which require ~1000 times higher sampling rates and high communication bandwidth. The fault location accuracy is not influenced by the fault

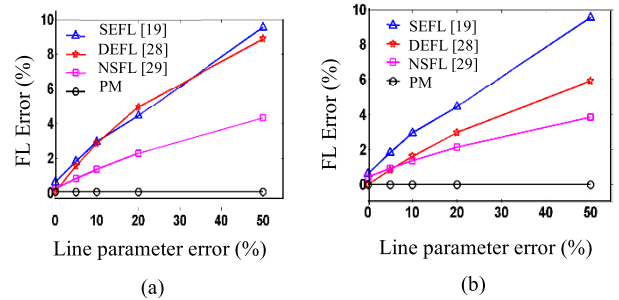


FIGURE 10. Comparative assessment of the proposed method vs practical methods for variation in the line parameters (a) a-g fault at 60km and (b) bc-g fault at 180km from Bus M.

resistance, fault type, line to source impedance ratio (SIRs), and loading of the line.

D. COMPARATIVE ASSESSMENT WITH PRACTICAL METHODS FOR VARIATION IN LINE PARAMETERS

The practically available single-ended [19] and double-ended [30], [31] methods need line parameters as an input. Any error in these parameters will affect the accuracy of the FL methods. Such inaccuracies may occur due to aging, temperature, sag of the conductor, etc., of the line. This section compares the proposed method with commercially established single-ended (SEFL) [19] and double-ended positive sequence (DEFL) [30] and double-ended negative sequence (NSFL) [31] methods. For this purpose, we have considered phase-to-ground (a-g) and phase-to-phase-ground (bc-g) faults at 60 and 180km from bus M respectively. The fault resistances considered for a-g and bc-g fault are 20 and 10Ω respectively.

Accuracy of the proposed method (PM) is assessed for different errors in the line parameters (resistance, inductance, capacitance) ranging from 0% to 50%. The evaluation results for a-g and bc-g fault cases are shown in Fig.10 (a) and (b) respectively.

From the figure, the fault location errors of both single-ended [19] and double-ended [30], [31] increases with increase in the error in line parameters whereas proposed method accuracy is independent on the parameter variation for both cases. For existing methods, the FL error is greater than 2% for variation of 10% in line parameters. This requires inspection of more towers and is time consuming for the existing methods. The FL accuracy claimed in existing methods is highly dependent on the accuracy of the line parameters.

E. COMPARATIVE ASSESSMENT WITH PRACTICAL METHODS FOR VARIATION IN SOURCE IMPEDANCES

Practically available single-ended [19] and double ended negative sequence-based methods [31] requires the two-port equivalent (source) impedance as a setting. These source impedances vary with structural and operational changes in power system. This section provides the performance of the available and proposed fault location methods for variation

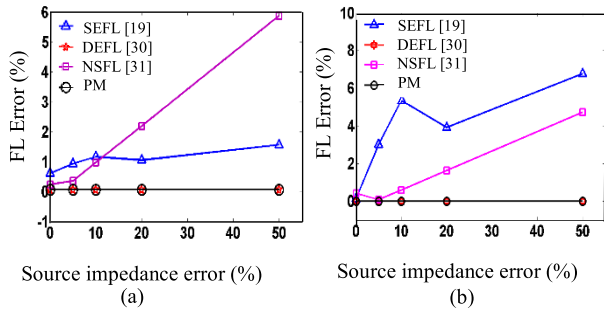


FIGURE 11. Comparative assessment of the proposed method vs practical methods for variation in the source impedance for (a) a-g fault at 50km and (b) bc-g fault at 150km from bus M.

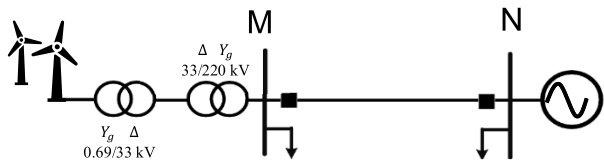


FIGURE 12. Two terminal line connected with CIRPP at bus M.

in source impedances. For this purpose, we have considered phase-to-ground (a-g) and phase-to-phase-ground (bc-g) faults at 50 and 150km from bus M respectively. The fault resistance for a-g and bc-g faults are 10 and 5Ω respectively.

Accuracy of the proposed method is verified for different errors in source impedances, ranging from 0% to 50%. The evaluation results for a-g and bc-g fault cases are shown in Fig. 11 (a) and (b) respectively. From the figure, the fault location accuracies of both single-ended [19] and double ended negative sequence [31] are increasing with increasing error in source impedance parameters whereas double-ended [30] and proposed method accuracies are independent of the source parameter variation for both cases. The single-ended method [19] is more sensitive with the source impedance angle variation and double-ended negative sequence-based method [31] sensitive with source impedance magnitude variation. The source strength is significantly varied with integration of the renewables into grid and the accuracy of these methods will further worsen for future power grids.

F. STUDY OF THE PROPOSED METHOD FOR LINES CONNECTED WITH RENEWABLE POWER PLANTS

This section provides the analysis of proposed and existing methods for lines connected with converter interfaced renewable power plants (CIRPPs). Two cases are considered such as renewable power plant at one side and both sides of the line.

1) CASE 1: TRANSMISSION LINE CONNECTED WITH RENEWABLE POWER PLANT AT ONE END OF THE LINE

Consider a two-terminal line with wind type IV renewable power plant connected at Bus M and N connected to power grid as shown in Fig.12. This configuration is very common

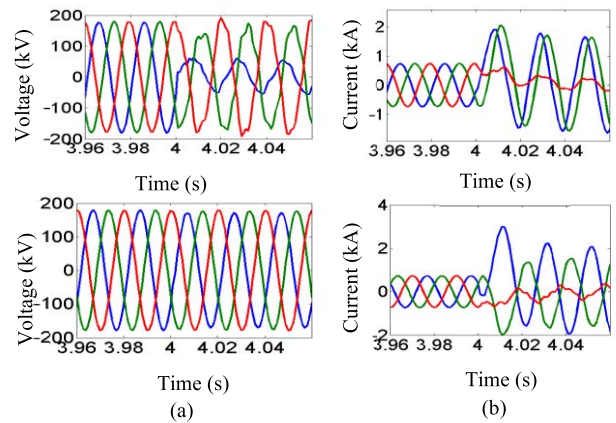


FIGURE 13. Pre and during fault voltage and current signals measured at (a) Bus M and (b) Bus N for a-g fault at 48km from M.

TABLE 5. Calculated line parameters using Π model.

Method	R^1 (Ω/KM)	L^1 (mH/KM)	C^1 (NF/KM)
Actual	0.1879	1.03870	16.18147
Proposed	0.1812	1.02750	16.26191
Error (%)	3.59	1.08	0.49

TABLE 6. Estimated line parameters using distributed line model.

Method	R^1 (Ω/KM)	L^1 (mH/KM)	C^1 (NF/KM)
Actual	0.1879	1.03870	16.18147
Proposed	0.1852	1.03891	16.17192
Error (%)	1.43	0.02	0.06

at the today’s situation of renewable power plant integration. Let us investigate the performance of proposed and existing methods for this configuration. Type IV wind turbine generator, which is a full converter model, with 200 units of 2MW each in compliance with various grid codes [23], [24] and the FRT characteristics are modeled for the study.

a: PROPOSED METHOD

Consider a-g fault at 48km from bus M on the transmission line with fault resistance of 50Ω, fault inception angle is 0°. The voltage and current wave forms are shown in Fig.13. From the figure, the current wave form is modulated, and voltage wave has more transients at wind farm side. The calculated (lumped model) and estimated (distributed line model) line parameters and corresponding errors compared to actual line parameters for this case are provided in the Table 5 and 6 respectively. From Table 5 and 6, the calculated and estimated parameters are close to actual parameters as for a line connected with a renewable resource. The calculated fault location using the estimated line parameters and post fault phasors is 48.24 km. The absolute percentage of fault location error is calculated using (31) is 0.1% for a 240 km transmission line for this case. The method is not affected by renewable integration.

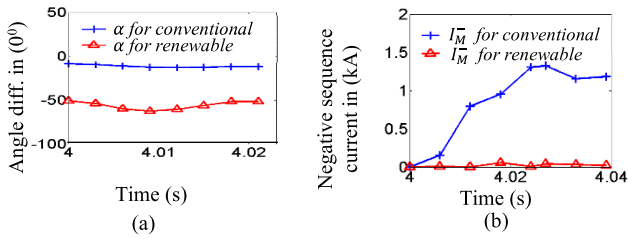


FIGURE 14. Shows (a) angle difference between fault current and IED measured current at bus M and (b) negative sequence current measured at Bus M for a-g fault at 48km from M.

b: SINGLE ENDED METHOD [19]

The calculated fault distance using single ended FL method [19] is 40.25 km. The absolute percentage of fault location error is calculated using (31) is 3.23% for a 240 km transmission line. The basic principle of single ended fault location depends on the accuracy of apparent impedance calculation. The apparent impedance for a a-g fault is obtained as in (32)

$$Z_{app} = \frac{V_{AM}}{I_{AM} + K_0 I_0} = Z_F + R_F \left(\frac{I_F}{I_{AM} + K_0 I_0} \right) \quad (32)$$

where V_{AM} , I_{AM} is phase A voltage and current phasors at M, I_0 is zero sequence current at M, Z_F is the line impedance till fault point, R_F is the fault resistance. Fig. 14(a) shows the angle difference (α) between fault current, I_F and IED measured current, $(I_{AM} + K_0 I_0)$. For comparison purposes, the figures include the respective plots when the CIRPPs at bus M is replaced by a conventional generation of same capacity. As seen from Fig.13(a) the value of α is higher (-56°) for the CIRPPs-connected system when compared to the conventional generation-connected system (-9°). To analyses the observations made, let us denote the term $\left(\frac{I_F}{I_{AM} + K_0 I_0} \right)$ in (32) as D. When α is very small, as in case of conventional generation-connected lines, D is mostly real. However, in CIRPPs-connected lines, since the current is controlled by the inverter control strategies, grid codes and FRT characteristics, α is high and consequently D is not real. This causes a significant negative reactance shift in apparent impedance estimated, which can potentially cause the IED at bus M calculates less impedance than actual value. Therefore, the single-ended fault location method [19] is calculates the fault location (40.25km) less than the actual value (48km) for this case.

c: DOUBLE ENDED METHOD [30]

The calculated fault location using double ended method [30] is 48.69 km. The absolute percentage of fault location error is calculated using (31) and it is 0.3% for this case. The double ended method is not impacted by the renewable integration; however, the accuracy of the method depends on the line parameter accuracy.

d: DOUBLE ENDED NEGATIVE SEQUENCE CURRENT BASED METHOD [31]

The negative sequence current measured at bus M for lines connected with renewable power plants and conventional

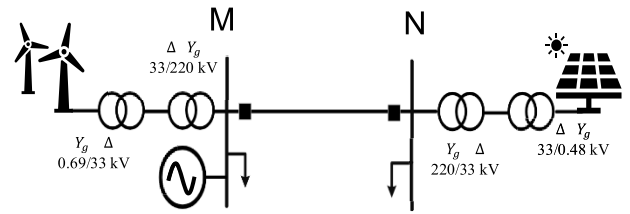


FIGURE 15. Line connected with CIRPP at both buses.

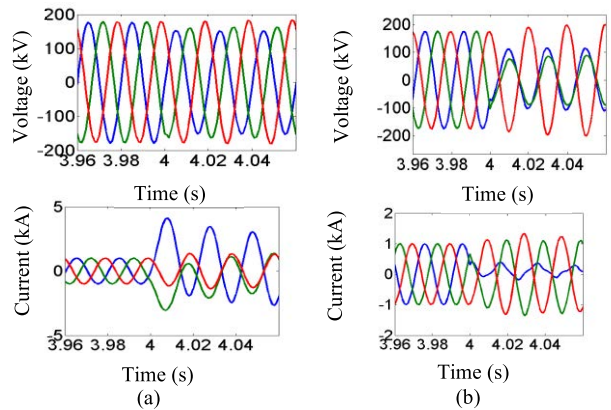


FIGURE 16. Pre and during fault voltage and current signals measured at (a) Bus M and (b) Bus N for a-g fault at 180km from M.

systems are shown in Fig 14. (b). From the figure, the negative sequence current measured for lines connected with renewable resources is almost zero and the method proposed in [31] will not work for this case. The most of the renewable power plants (wind type IV and Solar PV) will not produce negative sequence currents [23], [24]. Therefore, the method described in [31] may not work for full converter based [23], [24] (wind type IV and Solar PV) renewable resources.

2) CASE 2: TRANSMISSION LINE CONNECTED WITH RENEWABLE POWER PLANT AT BOTH ENDS OF THE LINE

Consider a transmission line with wind type IV renewable power plant connected at the Bus M and solar PV power plant connected at Bus N as shown in Fig.15. This configuration may be not practical today, however, this would be a possible situation in future. Let us investigate the performance of proposed and available FL methods for this configuration.

a: PROPOSED METHOD

Consider ab fault at 180km from bus M on the transmission line with fault resistance of 10Ω , fault inception angle is 60° . The voltage and current signals as shown in the Fig.16 for this case. The calculated and estimated parameters are tabulated in Table 7 and 8 respectively. From the Tables, the calculated and estimated parameters are close to actual parameters as in the case of line connected with a conventional resource. The calculated fault location using the estimated line parameters and post fault phasors is 179.48 km. The absolute percentage of fault location error is 0.2% for this case. The method

TABLE 7. Calculated line parameters using Π model.

Method	R^1 (Ω/KM)	L^1 (mH/KM)	C^1 (NF/KM)
Actual	0.1879	1.03870	16.18147
Proposed	0.1834	1.02722	16.25737
Error (%)	2.41	1.10	0.47

TABLE 8. Estimated line parameters using distributed line model.

Method	R^1 (Ω/KM)	L^1 (mH/KM)	C^1 (NF/KM)
Actual	0.1879	1.03870	16.18147
Proposed	0.1875	1.03862	16.16746
Error (%)	0.21	0.01	0.08

provides the desired result. Therefore, the proposed method is suitable for future renewable energy configurations.

b: SINGLE ENDED METHOD [19]

The calculated fault distance using single ended method [19] is 169.36 km. The absolute percentage of FL error for the case is 4.43%. The single ended fault location is not dependable for lines with CIRPPs connected at both ends.

c: DOUBLE ENDED METHOD [30]

Double ended method proposed in [30] is calculated the fault location is 179.32 km and absolute for this case is 0.2%. The method is not affected by the renewable integration at both sides of the line.

d: DOUBLE ENDED NEGATIVE SEQUENCE CURRENT BASED METHOD [31]

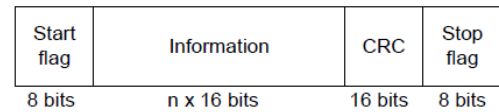
The negative sequence measurement-based method will not work for this situation as there is no significant negative sequence current available like previous case. And also, the method [31], requires the source impedance as an input. The source impedance for lines connected with renewable power plants varies continuously during the fault. The variation depends on the grid codes and inverter control systems [23], [24]. Therefore, this method may not give the accurate result when the lines are connected with CIRPPs.

G. SUMMARY OF COMPARATIVE ASSESSMENT

Identifying the best method for fault location also depends on the application scenario. For example, location estimates from two-ended algorithms are not always accurate as FL accuracy of these methods depends on the line parameters and data synchronization. Therefore, when implementing fault location methods, end users should be aware of the application scenario, identify possible error sources, and then choose the method that is robust to those error sources. The proposed method is not influenced by the most source of errors including lines connected with renewables whereas existing practically available methods influenced by many factors.

H. IMPLEMENTATION IN IED PLATFORM

The line differential protection is based on Kirchoff's law. A protection IED provides a phase segregated differential

**FIGURE 17. Data message structure.**

protection by comparing the currents entering and leaving the protected line [47]. Current from local end are connected to the analog input module or a transformer module of an IED. These are then digitized and forwarded as local end current to a differential protection function and to the remote end IED via Line Differential Communication Module (LDCM). Over the same LDCM, digitized current from remote end is received and forwarded to the differential.

In 64 kb mode, the format for communication is C37.94 and the data are exchanged every 5 ms. The transmitted data contains three currents and voltages, sent as sampled values, clock information, trip, block, and alarm signals. The data message as shown below.

In 2 Mb mode, the format for communication is still C37.94 and data sent every 1 ms i.e. telegrams are sent as soon as data is available. The data consists of nine analog sampled values and binary signals. The communication between the IED, can either be direct or via a multiplexer-telecommunication network interface. In either case, sampling of the analog values shall be synchronized in all IED to ensure proper functioning of the fault locator.

With networks using symmetric or fixed routes, echo-based synchronizing allows the internal clock in each local IED to act as a master and the internal clock in each remote IED operates as a slave. Time deviations between the internal clocks are monitored continuously and compensated for with echo messages between all ends at 40 ms intervals over the telecommunication network. With networks using unspecified route switching, reference for the internal clock comes from global time provided by, for example, a built-in GPS receiver. The internal clock in each IED [47] is thus set according to the GPS systems' global time. The maximum time deviation between internal clocks is set using a parameter MaxtDiffLevel in IED. If the actual time deviation is more than this parameter, the IED will not provide the fault location. There are two main types of telecommunication networks used by electric power utilities: Plesiochronous Digital Hierarchy (PDH) networks and Synchronous Digital Hierarchy (SDH). PDH networks are used with 64 kbps communication. Proper synchronization of PDH networks must be available so that they can be used with protection and fault location applications. SDH networks are used with 2 Mbps communication. The communication structure between the fault locators (IEDs) as shown in Fig.18.

IV. FIELD INSTALLATIONS AND EXPERIENCES

The proposed double ended fault location solution is implemented in IED and tested in laboratory. After success in

TABLE 9. Summary of factors effecting the fault location accuracy.

Method	Factors affecting fault location accuracy for existing and proposed method						
	Fault type	Fault Resistance	Source Impedance	Line Parameters	Data Synchronization	Mutual Compensation	Renewable Integration
SEFL[19]	Yes	Yes	Yes	Yes	No	Yes	Yes
DEFL[30]	No	No	No	Yes	Yes	No	No
NSFL[31]	Yes	No	Yes	Yes	No	No	Yes
PM	No	No	No	No	Yes	No	No

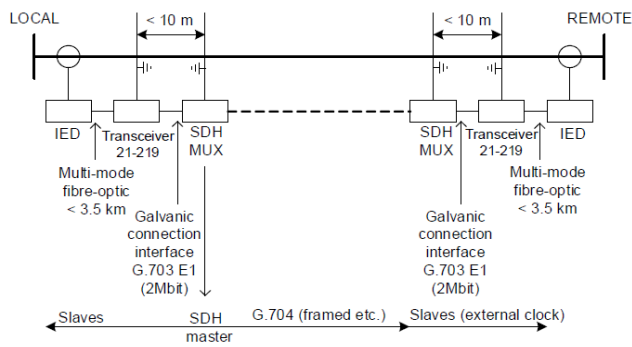


FIGURE 18. Communication structure between fault locator over SDH.

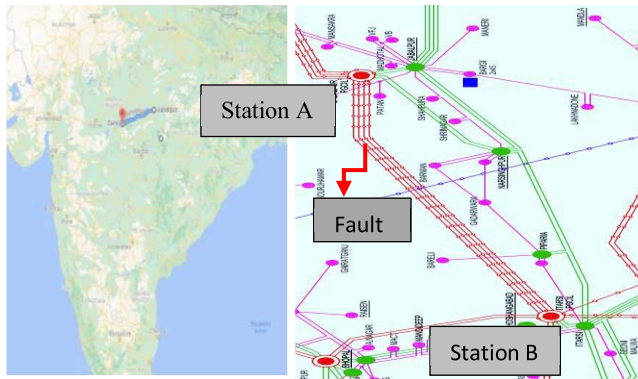


FIGURE 19. Pilot installation between station A and station B at power grid corporation of India limited (POWERGRID).

laboratory evaluation, the solution is installed on a 400-kV, 233.07 km line in Indian POWERGRID and on a 220-kV, 265.6 km line in Swedish Utility. Recently, two fault events were recorded in September 2021 on the transmission line where the solution is installed in the Indian system and one fault event on the line of Swedish installation in July 2021. The detail of the pilot experiences is described in following section.

A. PILOT 1: INDIAN PILOT INSTALLATION EXPERIENCE

A 400-kV, 233.07 km transmission line from Power Grid Corporation of India (POWERGRID) is chosen. The transmission line is in central part of India, and it connects between station A and B. The pilot installation setup is marked on

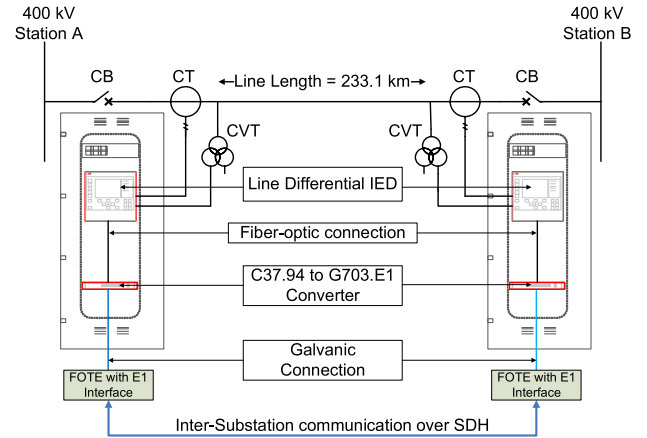


FIGURE 20. Pilot implementation setup at POWERGRID.

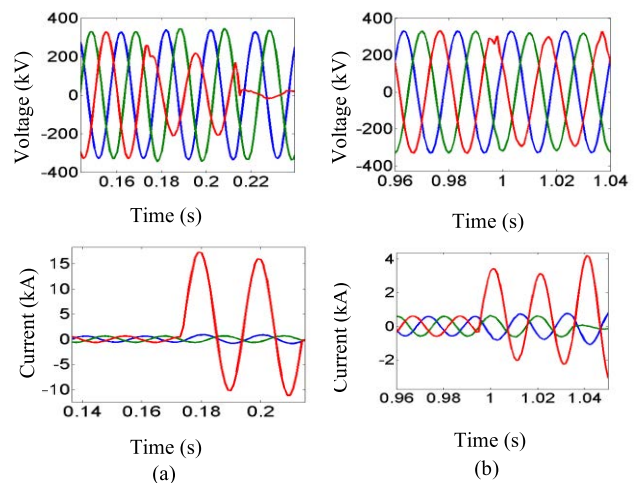


FIGURE 21. Pre and during fault voltage and current signals measured at (a) Station A and (b) Station B for c-g fault at 33km from station B for event 1.

the map and power network as shown Fig.19. The pilot setup including communication, configuration details are shown in Fig.20. Two fault events are recorded, and the details are provided below.

Fault event 1- Phase-c to-ground fault (c-g): The first fault occurred on 21st September 2021 and Fig.21 shows voltage and current signals recorded at station A and B terminals for

TABLE 10. Estimated line parameters using proposed method.

IED Location	R (Ω)	X (Ω)	B (MS)
STATION A	5.269	68.830	901.105
STATION B	5.288	68.795	900.621

TABLE 11. Calculated fault location using proposed method.

IED Location	Calculated Fault Location (Km)	Actual Fault Location (Km)	Error (%)
STATION A	32.87	33.00	0.05
STATION B	198.20	200.00	0.77

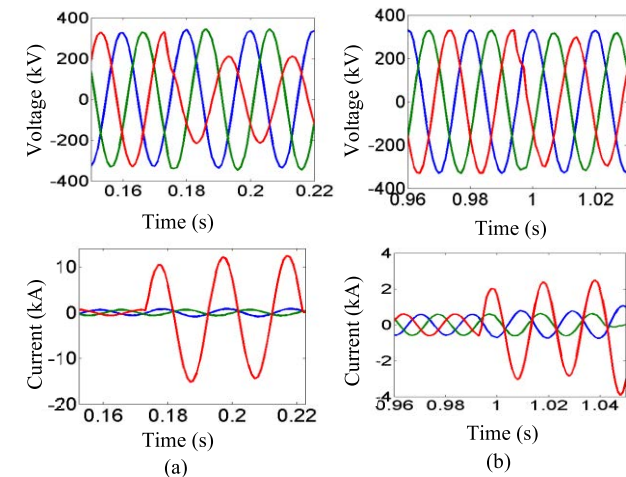


FIGURE 22. Pre and during fault voltage and current signals measured at (a) Station A and (b) Station B for c-g fault at 33km from station A Substation for event 2.

c-phase to ground fault. The line positive sequence parameters (resistance R), reactance X , and susceptance B) and fault location calculated by the IED at station A and station B are provided in Table 10 and 11 respectively. The estimated fault distance using the proposed method is 32.87km and 198.20km from station A and station B terminals respectively. When the line crew patrolled the line, they found a fault at 33km from station A. The difference of actual to estimated fault location is 130 meters or ± 1 tower span from the claimed value for this case. The line search required based on proposed method is two tower span distance for this case. The calculated line parameters can be used to update the protection settings.

Fault event 2- Phase-c to-ground fault: The second fault also occurred at same location as previous event and Fig.22 shows voltage and current signals recorded at station A and B terminals for this event. The line parameters and fault location calculated by the proposed method at station A and station B are provided in Table 12 and 13 respectively. The estimated fault distance using the proposed method is 33.23km and 200.80km from station A and B terminals respectively. The difference of actual to estimated fault location is 230 meters

TABLE 12. Estimated line parameters using proposed method.

IED Location	R (Ω)	X (Ω)	B (MS)
STATION A	5.026	68.721	901.658
STATION B	5.025	68.721	901.662

TABLE 13. Calculated fault location using proposed method.

IED Location	Calculated Fault Location (Km)	Actual Fault Location (Km)	Error (%)
STATION A	33.23	33.00	0.09
STATION B	200.80	200.00	0.34

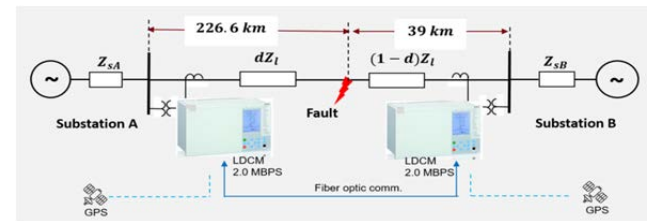


FIGURE 23. Pilot installation line of length 265.6km connected between station A and B at SVK, Sweden.

TABLE 14. Estimated line parameters using proposed method.

IED Location	R (Ω)	X (Ω)	B (MS)
STATION A	14.166	84.85	1000.548
STATION B	14.482	84.85	1000.865

or ± 1 tower span from the substation staff claimed value for this case.

Developed fault locator calculated and indicated the fault location as 32.87 km and 33.23, difference of only 130 and 230-meters differences respectively or ± 1 tower span from the claimed value in both cases. The line search required to locate the fault is only one tower span distance that significantly saves the line patrolling time and cost. The calculated line parameters are consistent for both cases and these parameters can be used to update the protection settings. The end customer (user) acknowledged that printed parameters are very valuable for relay settings and other power system monitoring applications.

B. PILOT 2: SWEDISH PILOT INSTATION EXPERIENCE

A 220-kV, 265.6 km transmission line chosen to install pilot at Swedish network. The line connects between Substation A and B as shown in Fig.23. In this pilot installation, the IED is configured with proposed double-ended solution and single-ended solution [19].

Fault event 1- Phase-a to-phase-b fault (ab): Double phase fault occurred on 14th July 2021 and Fig.24 shows the voltage and current recorded at station A and B for this event. The line parameters and fault location calculated by the IED (proposed

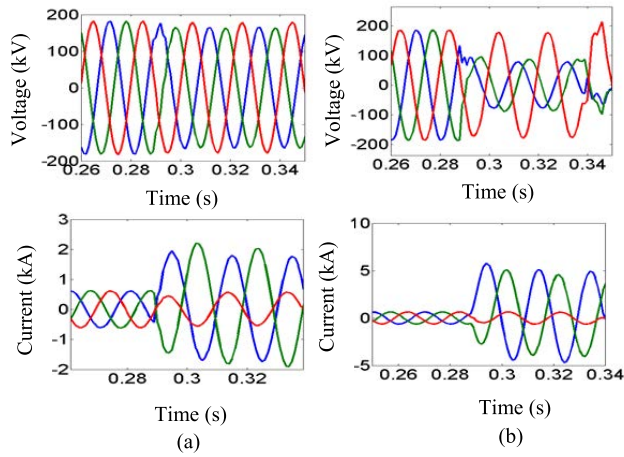


FIGURE 24. Pre and during fault voltage and current signals measured at (a) station A and (b) station B for ab fault at 226.6km from substation A.

TABLE 15. Calculated fault location using proposed method.

IED Location	Calculated Fault Location (Km)	Actual Fault Location (Km)	Error (%)
STATION A	226.82	226.60	0.08
STATION B	38.69	39.00	0.11

method) at both substations are provided in Table 14 and 15 respectively. The estimated fault distances using the proposed method are 226.82km and 38.69km from station A and B terminals respectively. When the line crew patrolled the line, they found a fault at 226.6 km and 39km from station A and B. The difference of actual to estimated fault location is 220 and 310 meters or ± 1 tower span from both the substations for this case. Calculated fault location using single-ended fault locator [19] are 248.6 and 40.37 km from station A and B respectively. After analysis and discussion with end customer, we concluded that the main reason for the higher FL errors (8.3% and 0.5% from station A and B respectively) of the SEFL [19] for this case is due to incorrect parameter settings.

V. CONCLUSION

In this work, a double-ended *setting-free* fault location method for transmission line connected with conventional or inverter based renewable resources is presented. The voltage and current signals from both terminals are the only inputs to the fault locator. The parameters of the line, or the source impedances at terminals are not required to be known which avoids the engineering effort and cost.

The performance of the method is evaluated using the EMTDC simulations. The simulation results show that the performance of the method is accurate for lines connected with conventional and renewable power plants for various fault scenarios. The results are not affected by the renewable integration whereas negative sequence based double ended, and single-ended method fail or inaccurate for the lines connected with renewable power plants. The accuracy

TABLE 16. Source impedances.

Sequence	Terminal A-end	Terminal B-end
Positive	$3.80 + j30.9 \Omega$	$2.80 + j26.0 \Omega$
Negative	$3.80 + j30.9 \Omega$	$2.80 + j26.0 \Omega$
Zero	$7.17 + j52.65 \Omega$	$6.2 + j48.546 \Omega$

of the method is compared to practically available methods for impact of error in line and source parameters. For the available methods, the fault location error increases for higher inaccuracies in line parameters whereas, the proposed method is independent of these parameter changes.

The proposed method is implemented in existing line protection IED using 1kHz sampling rate. The proposed method does not require information about line parameters or settings, saves on engineering cost and does not require any additional hardware beyond what is required for a modern line differential protection solution, i.e., a 2 Mbps communication link. The method is installed at Indian and Swedish power system, the early field results confirm the validity of the method. The field experimental results are matching with simulation results. It helped in pilot installation to locate the faults within one tower span distance which in-turn aids in quick restoration of the power supply. Quick restoration of power supply reduces customer complaints, outage time, and therefore minimizes revenue loss, outage management costs for utilities and the end users. These geographically diverse pilot installation results stand as testimony to the accuracy of the developed fault location method.

In a more general testing, where different fault conditions are considered, the fault location error in majority of cases is $\sim 0.1\%$. Based on these results and confirmation from the pilot installations it is expected that the fault location accuracy will be within 2 tower spans even in more problematic situations with higher fault resistances and different fault types. The innovative and accurate line parameter estimation in the proposed method enables achievement of accuracy levels comparable to the traveling wave fault locator technology that uses 1000 times higher sampling frequency, more costly hardware and commissioning process. The solution is suitable to locate the fault in different geographical regions (example, snowy areas, coastal, hilly terrains, deserts, etc.) as it is independent of the transmission line parameters (which change with atmospheric conditions). Further, the calculated parameters of the line can be used for protection and power system monitoring application settings.

As a future work, the proposed model-free approach can be implemented in SCADA/EMS control centers or cloud-based platforms. Setting-free fault location for three terminal and non-homogeneous/mixed (combined overhead and underground cable) circuits is difficult as the impedance parameters are not same for all sections. This work can be extended for these complex power networks. The issues with data synchronization and measurement errors can be eliminated in future works.

APPENDIX

See Table 16.

ACKNOWLEDGMENT

The authors express gratitude to Power Grid Corporation of India Ltd. (POWERGRID), India, for their support and cooperation during the installation of IEDs with double-ended fault locator in their substations. Their valuable and timely inputs have enabled in validation of the performance of proposed double ended fault locator solution. And also, they express gratitude to Svenska Kraftnat (SVK) Team for their continuous support for experimenting the double ended fault locator solution.

REFERENCES

- [1] M. M. Saha, J. Izykowski, and E. Rosolowski, *Fault Location on Power Networks* (Power Systems). London, U.K.: Springer, 2010.
- [2] *IEEE Guide for Determining Fault Location on AC Transmission and Distribution Lines*, Standard C37.114–2014 (Revision of IEEE Std C37.114–2004), IEEE, Jan. 2015, pp. 1–76.
- [3] H. Panahi, R. Zamani, M. Sanaye-Pasand, and H. Mehrjerdi, “Advances in transmission network fault location in modern power systems: Review, outlook and future works,” *IEEE Access*, vol. 9, pp. 158599–158615, 2021.
- [4] E. O. Schweitzer, A. Guzman, M. V. Mynam, V. Skendzic, B. Kasztenny, and S. Marx, “Locating faults by the traveling waves they launch,” in *Proc. 67th Annu. Conf. Protective Relay Eng.*, Mar. 2014, pp. 95–110.
- [5] A. Guzman, B. Kasztenny, Y. Tong, and M. V. Mynam, “Accurate and economical traveling-wave fault locating without communications,” in *Proc. 71st Annu. Conf. Protective Relay Eng. (CPRE)*, College Station, TX, USA, Mar. 2018, pp. 1–18.
- [6] C. Zhang, G. Song, T. Wang, and L. Yang, “Single-ended traveling wave fault location method in DC transmission line based on wave front information,” *IEEE Trans. Power Del.*, vol. 34, no. 5, pp. 2028–2038, Oct. 2019.
- [7] H. Shu, X. Liu, and X. Tian, “Single-ended fault location for hybrid feeders based on characteristic distribution of traveling wave along a line,” *IEEE Trans. Power Del.*, vol. 36, no. 1, pp. 339–350, Feb. 2021.
- [8] O. D. Naidu and A. K. Pradhan, “Precise traveling wave-based transmission line fault location method using single-ended data,” *IEEE Trans. Ind. Informat.*, vol. 17, no. 8, pp. 5197–5207, Aug. 2021.
- [9] F. V. Lopes, K. M. Silva, F. B. Costa, W. L. A. Neves, and D. Fernandes, “Real-time traveling wave-based fault location using two-terminal unsynchronized data,” in *IEEE Trans. Power Del.*, vol. 30, no. 3, pp. 1067–1076, Jun. 2015.
- [10] F. V. Lopes, P. Lima, J. P. G. Ribeiro, T. R. Honorato, K. M. Silva, E. J. S. Leite, W. L. A. Neves, and G. Rocha, “Practical methodology for two-terminal traveling wave-based fault location eliminating the need for line parameters and time synchronization,” *IEEE Trans. Power Del.*, vol. 34, no. 6, pp. 2123–2134, Dec. 2019.
- [11] *Qualitrol Traveling Wave Locator and Monitor*. Accessed: Sep. 2016. [Online]. Available: https://www.qualitrolcorp.com/wp-content/uploads/2016/09/IP-F21-02L-01E_TWS_FL8_FL1.pdf
- [12] *Reason RPV311 Digital Fault Recorder With Fault Location and PMU*. Accessed: May 2018. [Online]. Available: <https://www.gegridsolutions.com/products/brochures/reason%20rpv311-brochure-en-2018-05-33113-a4.pdf>
- [13] O. Naidu and A. K. Pradhan, “A traveling wave-based fault location method using unsynchronized current measurements,” *IEEE Trans. Power Del.*, vol. 34, no. 2, pp. 505–513, Oct. 2018.
- [14] O. D. Naidu and A. K. Pradhan, “Model free traveling wave based fault location method for series compensated transmission line,” *IEEE Access*, vol. 8, pp. 193128–193137, 2020.
- [15] E. O. Schweitzer III, M. V. Mynam, A. Guzman-Casillas, V. Skendzic, B. Z. Kasztenny, and D. E. Whitehead, “Power line parameter adjustment and fault location using traveling waves,” U.S. Patent 8990036 B1, Mar. 24, 2015.
- [16] T. Takagi, Y. Yamakoshi, M. Yamaura, R. Kondow, and T. Matsushima, “Development of a new type fault locator using the one-terminal voltage and current data,” *IEEE Power Eng. Rev.*, vol. PER-2, no. 8, pp. 59–60, Aug. 1982.
- [17] L. Eriksson, M. M. Saha, and G. D. Rockefeller, “An accurate fault locator with compensation for apparent reactance in the fault resistance resulting from remote-end infeed,” *IEEE Trans. Power App. Syst.*, vol. PAS-104, no. 2, pp. 423–436, Feb. 1985.
- [18] L. Ji, X. Tao, Y. Fu, Y. Fu, Y. Mi, and Z. Li, “A new single ended fault location method for transmission line based on positive sequence superimposed network during auto-reclosing,” *IEEE Trans. Power Del.*, vol. 34, no. 3, pp. 1019–1029, Jun. 2019.
- [19] *Hitachi Energy Line Distance Protection REL670 Manual*. [Online]. Available: <https://search.abb.com/library/Download.aspx?DocumentID=1MRK506372-BEN&LanguageCode=en&DocumentPartId=&Action=Launch>
- [20] O. E. Schweitzer, “A review of impedance-based fault locating experience,” *Proc. 15th Annu. Western Protective Relay Conf.*, Spokane, WA, USA, Oct. 1988, pp. 24–27.
- [21] S. Das, S. Santoso, A. Gaikwad, and M. Patel, “Impedance-based fault location in transmission networks: Theory and application,” *IEEE Access*, vol. 2, pp. 537–557, 2014.
- [22] A. L. Dalcastagne and S. L. Zimath, “A study about the sources of error of impedance-based fault location methods,” in *Proc. IEEE/PES Transmiss. Distrib. Conf. Expo., Latin Amer.*, Bogota, Colombia, Aug. 2008, pp. 1–6.
- [23] A. Hooshyar, M. A. Azzouz, and E. F. El-Saadany, “Distance protection of lines emanating from full-scale converter-interfaced renewable energy power plants—Part I: Problem statement,” *IEEE Trans. Power Del.*, vol. 30, no. 4, pp. 1770–1780, Aug. 2015.
- [24] S. Paladhi and A. K. Pradhan, “Adaptive distance protection for lines connecting converter-interfaced renewable plants,” *IEEE J. Emerg. Sel. Topics Power Electron.*, vol. 9, no. 6, pp. 7088–7098, Dec. 2021.
- [25] N. George and O. D. Naidu, “Distance protection issues with renewable power generators and possible solutions,” in *Proc. 16th Int. Conf. Develop. Power Syst. Protection (DPSP)*, Mar. 2022, pp. 1–6.
- [26] P. Chang, G. Song, J. Hou, and R. Xu, “A single-ended fault location method for grid-connected converter system based on control and protection coordination,” *IEEE Trans. Power Del.*, vol. 37, no. 4, pp. 3071–3081, Aug. 2022.
- [27] P. Chang, G. Song, J. Hou, and R. Xu, “A single-terminal fault location method for transmission lines integrated by inverter-type source,” *IEEE Trans. Power Del.*, vol. 37, no. 3, pp. 1704–1713, Jun. 2022.
- [28] A. A. Girgis, D. G. Hart, and W. L. Peterson, “A new fault location technique for two-and three-terminal lines,” *IEEE Trans. Power Del.*, vol. 7, no. 1, pp. 98–107, Jan. 1992.
- [29] C.-W. Liu, T.-C. Lin, C.-S. Yu, and J.-Z. Yang, “A fault location technique for two-terminal multisession compound transmission lines using synchronized phasor measurements,” *IEEE Trans. Smart Grid*, vol. 3, no. 1, pp. 113–121, Mar. 2012.
- [30] T.-C. Lin, J.-Z. Yang, C.-S. Yu, and C.-W. Liu, “Development of a transmission network fault location platform based on cloud computing and synchrophasors,” *IEEE Trans. Power Del.*, vol. 35, no. 1, pp. 84–94, Feb. 2020.
- [31] D. A. Tziouvaras, “New multi-ended fault location design for two-or three-terminal lines,” in *Proc. 7th Int. Conf. Develop. Power Syst. Protection (DPSP)*, 2001, pp. 395–398.
- [32] H. Torkaman, E. Zeraatkar, N. Deyhimi, H. H. Alhelou, and P. Siano, “Rearrangement method of reducing fault location error in tied uncompleted parallel lines,” *IEEE Access*, vol. 10, pp. 51862–51872, 2022.
- [33] C. Galvez and A. Abur, “Fault location in power networks using a sparse set of digital fault recorders,” *IEEE Trans. Smart Grid*, vol. 13, no. 5, pp. 3468–3480, Sep. 2022, doi: 10.1109/TSG.2022.3168904.
- [34] B. R. Jeffrey, B. Gabriel, and T. Dmetrios, “Multi-ended fault location system,” U.S. Patent 6256592 B1, Jul. 3, 2001.
- [35] J. P. William, Z. K. Bogdan, and G. A. Mark, “Multi-ended fault location system,” U.S. Patent 7472026 B2, Dec. 30, 2008.
- [36] G. L. Kusic and D. L. Garrison, “Measurement of transmission line parameters from SCADA data,” in *Proc. IEEE PES Power Syst. Conf. Expo.*, New York, NY, USA, Oct. 2004, pp. 440–445.
- [37] Y. Wang, W. Xu, and J. Shen, “Online tracking of transmission-line parameters using SCADA data,” *IEEE Trans. Power Del.*, vol. 31, no. 2, pp. 674–682, Apr. 2016.
- [38] L. Zhang and A. Abur, “Identifying parameter errors via multiple measurement scans,” *IEEE Trans. Power Syst.*, vol. 28, no. 4, pp. 3916–3923, Nov. 2013.
- [39] M. Asprou and E. Kyriakides, “Identification and estimation of erroneous transmission line parameters using PMU measurements,” *IEEE Trans. Power Del.*, vol. 32, no. 6, pp. 2510–2519, Dec. 2017.

- [40] Y. Liao and M. Kezunovic, "Online optimal transmission line parameter estimation for relaying applications," *IEEE Trans. Power Del.*, vol. 24, no. 1, pp. 96–102, Jan. 2009.
- [41] O. D. Naidu, N. George, and P. Yalla, "Parameter estimation, selective auto-reclosing and fault location for three-terminal mixed transmission lines using synchronised data," *IET Gener., Transmiss. Distrib.*, vol. 14, no. 25, pp. 6049–6060, Dec. 2020.
- [42] D. Ritzmann, P. S. Wright, W. Holderbaum, and B. Potter, "A method for accurate transmission line impedance parameter estimation," *IEEE Trans. Instrum. Meas.*, vol. 65, no. 10, pp. 2204–2213, Oct. 2016.
- [43] A. Bendjabeur, A. Kouadri, and S. Mekhilef, "Novel technique for transmission line parameters estimation using synchronised sampled data," *IET Gener., Transmiss. Distrib.*, vol. 14, no. 3, pp. 506–515, Feb. 2020.
- [44] A. K. Gautam, S. Majumdar, and H. Parthasarathy, "State and parameter estimation of non-uniform transmission line using Kronecker product based modeling," *IEEE Trans. Power Del.*, early access, Feb. 7, 2022, doi: [10.1109/TPWRD.2022.3149137](https://doi.org/10.1109/TPWRD.2022.3149137).
- [45] J. Sun, Q. Chen, and M. Xia, "Data-driven detection and identification of line parameters with PMU and unsynchronized SCADA measurements in distribution grids," *CSEE J. Power Energy Syst.*, early access, May 6, 2022, doi: [10.17775/CSEEJPES](https://doi.org/10.17775/CSEEJPES).
- [46] O. Naidu, P. Yalla, A. Sai, and S. Sawai, "Model-free fault location for transmission lines using phasor measurement unit data," *CIGRE Study Committee B5 Colloq.*, vol. 5, pp. 1–12, Jun. 2019.
- [47] *Hitachi Energy Product Guide, Line Differential Protection RED6702.1*. [Online]. Available: <https://search.abb.com/library/Download.aspx?DocumentID=1MRK505346-BEN&LanguageCode=en&DocumentPartId=&Action=Launch>



A. V. S. R. SAI received the master's degree in power systems from the National Institute of Technology (NIT), Tiruchirappalli, India, in 2007. He is currently working as a Senior Research and Development Engineer with Hitachi Energy, Grid Automation Research and Development. He joined the ABB Research and Development Center, Bengaluru, in 2007, as a Domain Engineer. He is involved in the development of relay application function library (AFL) related to line protection and monitoring. His research interests include power system protection and monitoring applications and specialized in fault location.



A. N. PRAVEEN received the B.E. degree in electrical and electronics from the National Institute of Engineering, Mysuru, India, in 2009. He is currently pursuing the Ph.D. degree in protection applications for smart grid with the Indian Institute of Technology (IIT), Madras, India. He joined ABB, in 2009, and worked as a Commissioning Engineer for UHV and EHV substations and then as a Senior Application Engineer for grid automation systems. He is currently working as the Technical Support Line Manager with Hitachi Energy, Grid Automation Products.



O. D. NAIDU (Senior Member, IEEE) received the Ph.D. degree from the Indian Institute of Technology (IIT), Kharagpur, India. From 2009 to 2012, he was a Senior Power System Application Development Engineer at the ABB India Development Center, Bengaluru, India. From 2012 to 2019, he was the Principal Scientist at the ABB Corporate Research Center, Bengaluru. He is currently working as a Senior Principal Engineer with Hitachi Energy, Grid Automation Research and Development, Bengaluru. He is the author of more than 50 scientific papers and 40 patent applications. He holds 15 granted patents. His research interests include power system protection, fault location, renewable integration and monitoring, artificial intelligence applications to power system protection, and monitoring.



PATRICK COST joined ABB, the Netherlands, in 2006, where worked on various projects as a Product and Project Engineer. From 2010 to 2015, he was an Application Specialist and the Regional Technical Marketing Manager for the Central Europe and Sub-Sahara Africa, Vasteras, Sweden. In 2015, he joined the Global Product Management Team for bay level products, with a focus on protection application development. He is currently the Global Product Manager with Hitachi Energy, Vasteras.



SINISA ZUBIC received the Ph.D. degree from the University of Belgrade, Serbia, in 2013. From 2014 to 2018, he joined ABB, where he was a Senior Scientist at the ABB Corporate Research Center, Poland. Before joining ABB, he was a Teaching and Research Assistant at the Faculty of Electrical Engineering, Banja Luka, Bosnia and Herzegovina. He is currently the Research and Development Manager in application software at Hitachi Energy, Vasteras, Sweden.



HÅKAN ERIKSSON received the B.S. degree in computer science from the University of Uppsala, Sweden, in 1990. He was worked at ASEA and ABB in various positions related to relay protection systems including test and RTDS simulation, research and development, technical support, and lead engineer for over 32 years (1977–2010). Since 2010, he has been working with the Swedish TSO Svenska kraftnät as a Relay Protection Engineer.